Biocybernetics and Biomedical Engineering
2008, Volume 28, Number 4, pp. 59–73

Correction of Anisotropy Coefficient in Original Henyey Greenstein Phase Function for Monte Carlo Simulations of Light Transport in Tissue

NORBERT S. ŻOŁEK*, STANISŁAW WOJTKIEWICZ, ADAM LIEBERT

* *Institute of Biocybernetics and Biomedical Engineering, Polish Academy of Sciences, Warsaw, Poland*

In this paper, two different methods for calculation of polar deflection angle are compared. The scattering angle is defined by numerical inversion of cumulative distribution of the original Henyey-Greenstein phase function. Results of the Monte Carlo simulations obtained in this manner are compared with results of simulations in which the analytical inversion of the probability density for the cosine of the deflection angle is applied. Investigations are carried out for media with optical properties similar to these typical for living tissues as well for very small source detector separations (50–500 μm), i.e. in conditions, in which the diffusion theory can not be applied. The distributions of visiting probability of photons penetrating into the semi-infinite medium are obtained for various methods of phase function calculation. It can be observed that the methods of calculation of polar deflection angle influence significantly spatial distributions of reflectance and visiting probability obtained by Monte Carlo simulations. The approximated transformation of the anisotropy coefficient used in simulations carried out with the use of the original Henyey-Greenstein function to effective anisotropy coefficient is presented; that makes possible comparisons of the results of Monte Carlo simulations obtained by using different methods.

K e y w o r d s: Monte Carlo, phase function, light transport

1. Introduction

The Monte Carlo method is frequently used in modeling of light propagation in turbid media [1–11]. The method can be applied for complicated boundary conditions, which are difficult to analyze using radiative transport equation [3, 12]. The Monte Carlo simulations are used particularly for complicated nonhomogeneous media with nonisotropic scattering and in the cases of small source–detection separations,

* Correspondence to: Norbert S. Żołek, Institute of Biocybernetics and Biomedical Engineering, Polish Academy of Sciences, ul. Ks. Trojdena 4, 02-109 Warsaw, Poland, e-mail: norbert@ibib.waw.pl
Received 30 January 2008; Accepted 18 August 2008

i.e. in situations, for which diffusion equation approach is improper [13, 14, 15]. The method can be also applied for modeling of fluorescence processes [11, 16] and quasi-elastic Doppler scattering [5, 17].

Monte Carlo modeling of light propagation is based on calculation of the single photon paths in a medium, the optical properties of which can be determined by the absorption and scattering coefficients (μ_a and μ_s). The trajectory of photon consists of straight segments between the consecutive scattering events. The distance between the two scattering events, called free pathlength, is randomly sampled by an exponential distribution dependent on both absorption coefficient μ_a and scattering coefficient μ_s. After every scattering event, a new direction for the photon propagation, represented by the directional cosines, can be determined. The azimuthal angle is calculated using the random number with the uniform distribution in the range $[0;2\pi)$. Probability distribution of the polar deflection angle can be approximated by the Henyey-Greenstein (HG) phase function of the following form:

$$p(\phi) = \frac{1-g^2}{2(1+g^2-2g\cos(\phi))^{3/2}}, \tag{1}$$

where $\phi \in [0;\pi]$ is the polar deflection angle (Fig. 1) and $g \in [-1;1]$ – anisotropy coefficient. This function is used to describe scattering of light in galaxies [18], but it also allows to approximate scattering of light in living tissues [19, 20]. The HG phase function describes the probability of the polar deflection angle after each scattering event. The event depends on anisotropy coefficient g, which is equal to the mean cosine of scattering angle, i.e. $g = \langle\cos(\phi)\rangle$. To determine the random number, distributed according to the phase function (eq. 1), the probability integral transform [21] is commonly used. This method requires determination of the random variables with uniform distribution $u \in [0,1]$, and the transformation $x = F^{-1}(u)$, where F is the cumulative distribution of phase function.

It is worth noting that, when the function (eq. 1) is interpreted directly as a probability density function of polar deflection angle for the Monte Carlo simulations, the obtained distribution of polar deflection angle is not correct for isotropic scattering [22].

Definition of the directional cosines of a new direction of the photon requires calculation of at least cosine of the polar deflection angle and cosine of azimuthal angle [23]. Such an operation is, however, time consuming, especially in such highly scattering media as tissues; it is because of large number of occurring scattering events [23]. The definition (eq. 1) integrated over solid angle gives the probability distribution of the form [18]:

$$p(\phi) = \frac{\left(1-g^2\right)\sin(\phi)}{2(1+g^2-2g\cos(\phi))^{3/2}}, \tag{2}$$

which is analogous to probability of the cosine of angle [24] (not the angle values as in (eq. 1)):

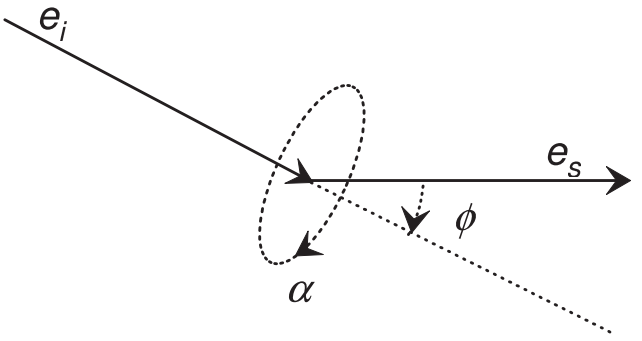

Fig. 1. Scheme of scattering event with polar deflection angle (ϕ) and azimuthal angle (α). Incident direction – e_i, direction after scattering e_s

$$p(\eta) = \frac{1-g^2}{2(1+g^2-2g\eta)^{3/2}}, \tag{3}$$

where $\eta = \cos(\phi)$. This form of the HG phase function (eq. 3) allows to derive the analytical inversion of cumulative distribution and leads to direct calculation of the cosine of the polar deflection angle [24]. This approach was implemented in the MCML code [25, 26], and is commonly used for modeling of light transport in tissues.

Recently, Binzoni et al. [22] reported on differences in the spatial distribution of reflectance obtained by the Monte Carlo simulations at large source-detector separations. The calculations were carried out using different HG phase function definitions.

The aim of our study was to compare the spatial distributions of reflectance at small source-detector separations. To this end, the transformation of the anisotropy coefficient to effective anisotropy coefficient is derived. The anisotropy coefficient was applied in the calculation of deflection angle using the original HG function (eq. 1). Such an approach makes possible analysis of the results obtained by the Monte Carlo simulations for different definitions of the HG phase function.

2. Theoretical Background

2.1. Probability Density Function Calculated Using the Original Hanyey-Greenstein Function

The probability density function describing the polar deflection angle was defined in [18] by equation (1). The cumulative distribution of (eq. 1) can be defined as :

$$F_\phi(x) = \int_0^x p(\varphi)d\varphi, \tag{4}$$

where $x \in [0;\pi]$. Inversion of $F_\phi(x)$ cannot be obtained analytically. Only the numerical inversion of cumulative distribution of the original HG phase function based on the look-up tables with an additional linear interpolation between two neighboring points can be performed. This procedure enables calculation of the cosine of random angle ϕ by equation (5):

$$c(\phi) \overset{def}{=} \cos(\phi) = \cos(F_\phi^{-1}(\xi)). \tag{5}$$

2.2. Probability Density Function of the Cosine of Polar Deflection Angle

The definition proposed in [24] gives a direct probability distribution of the cosine of polar deflection angle (eq. 2). In comparison to the probability of this angle, it has the cumulative distribution in the form:

$$F_c(x) = \int_{-1}^{x} p(\cos(\phi))d\cos(\phi)\,. \tag{6}$$

For this distribution, the inverse function can be obtained analytically:

$$c_a(\phi) \overset{def}{=} \cos(\phi) = \begin{cases} \dfrac{1}{2g}\left(1+g^2-\left(\dfrac{1-g^2}{1-g+2g\xi}\right)^2\right) & \text{if} \quad g \neq 0 \\ 2\xi - 1 & \text{if} \quad g = 0 \end{cases} \tag{7}$$

This method of calculation of the cosine of polar deflection angle was implemented into the MCML code [25, 26].

2.3. Correction of the Cosine of Polar Deflection Angle

The accuracy of definition (eq. 1) was examined by fitting the function $c_a(\phi)$ (eq. 7) to the data sampled from the distribution of cosine defined by $c(\phi)$ (eq. 5). In order to fit the cosine function to the sampled data, a small modification of the definition of $F_\phi(x)$ (eq. 4) was necessary. The function $c_a(\phi)$ returns values of the cosine corresponding to the values of cosine for angles $[\pi;2\pi]$. To provide the same increasing parts of the cosine function in the both cases, the cumulative distribution $c(\phi)$ (eq. 4) takes the form:

$$F_s(x) = \int_{\pi}^{x} p(\varphi)d\varphi\,, \tag{8}$$

where $x \in [\pi;2\pi]$.

The 1000 sampled values of $F_s^{-1}(\xi)$ were used to calculate $c(\phi)$ for the fitting procedure. Anisotropy coefficient g_a in analytical expression $c_a(\phi)$ was chosen to minimize the root mean square error between analytical expression $c_a(\phi)$ and the results of numerical inversion of cumulative distribution of the original HG phase function $c(\phi)$.

3. Monte Carlo Code for Simulation of Light Transport

The weighted Monte Carlo algorithm implemented for this work is based on the MCML code [25, 26]. The code was modified to collect additional information about each trajectory of the photons. Due to the radial symmetry around the source axis, the photons escaping from the medium are collected within the ring shaped detection areas. Detailed information about the trajectories was used to determine the spatial distribution of the visiting probability, which is defined as the probability that the photon visits a voxel during its travel from the point of its injection to the point of its escape.

The photon trajectories were rotated around the source axis to have the source position and all the detection positions on a one plane. After the rotation, the detection area became a one-dimensional section (of a length equal to the thickness of the detection ring) instead of the ring. The trajectories were projected onto the 2D plane perpendicular to the surface of the medium and crossing the source and the detection positions. The projection plane was divided into pixels of the fixed size, and the trajectories were drawn in the 2-dimensional space of the pixels as straight lines between the consecutive scattering events using the Bresenham algorithm of the line drawing [27]. Each trajectory was added to the distribution with its weight equal to the weight of the respective detected photon. By normalizing to maximal value the visiting probabilities of the simulated medium by the photons were obtained. The number of the emitted photons in each case was 2×10^7. The thickness of the ring shaped detection areas was 5 μm.

The projection plane was divided into pixels of a size equal to *3r/200* each (where *r* is source-detector separation). The size of the projection plane was 3 times larger than the source-detector separation distance in the horizontal direction and 4 times larger than the source-detector separation in the vertical direction.

The calculation of the polar deflection angles was performed using two definitions of the HG function: generating the polar deflection angle according to the distribution (eq. 1), and generating the cosine of polar deflection angle in accordance with the original MCML code (eq. 2).

The C language code was compiled using the gnu c compiler (http://gcc.gnu.org/). The simulations were run on a PC class computer (AMD AthlonX2 4800) under control of the “Windows XP” operating system.

4. Results

The differences between the values of the cosine of polar deflection angle generated by the analytical expression $c_a(\phi)$ and the cosine $c(\phi)$ generated by the direct inversion using formula (eq. 5) for various g are shown in Fig. 2. Figure 2A represents distributions of the cosine for $g = 0$ and Fig. 2B represents distributions for $g = 0.2$,

0.5, 0.8, 0.9, 0.95, 0.995. The solid depict the numerically calculated distribution of the cosine of polar deflection angle $c(\phi)$. The dashed lines show the distributions of the cosine of polar deflection angle obtained on the basis of analytical inversion $c_a(\phi)$. The differences of the obtained distributions are large for all anisotropy coefficients g. Figure 2A shows how analytical inversion $c_a(\phi)$ for the isotropic scattering differs from the cosine values obtained on the basis of numerical inversion $c(\phi)$.

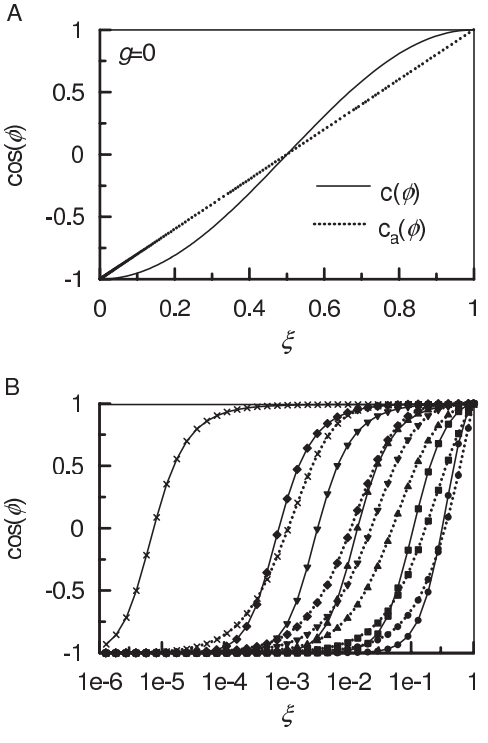

Fig. 2. Distributions of the cosine of polar deflection angle for different anisotropy coefficients obtained by the analytical inversion $c_a(\phi)$ (eq. 7) – dotted lines, distributions obtained by the numerical inversion $c(\phi)$ (eqns. 5, 8) – solid lines. A: obtained for isotropic scattering – $g = 0$; B: obtained for anisotropic scattering $g = 0.2$ – ●, $g = 0.5$ – ■, $g = 0.8$ – ▲, $g = 0.9$ – ▼, $g = 0.95$ – ◆, $g = 0.995$ – ✱

The differences of the photon directions densities within a unit sphere after scattering event are presented in Fig. 3 for different anisotropy coefficients. The direction of incident photons is parallel to z axis and scattering event occurs at the origin. Number of simulated photons is 10000. The photon direction density of isotropic scattering is presented in the upper row of Figure 3. As expected from theory, when the function (eq. 1) is directly interpreted as a probability density function of polar deflection angle for the Monte Carlo simulations, it does not give correct distribution in the case of isotropic scattering. This phenomena can be observed in differences between distributions presented in the upper row in Fig. 3.

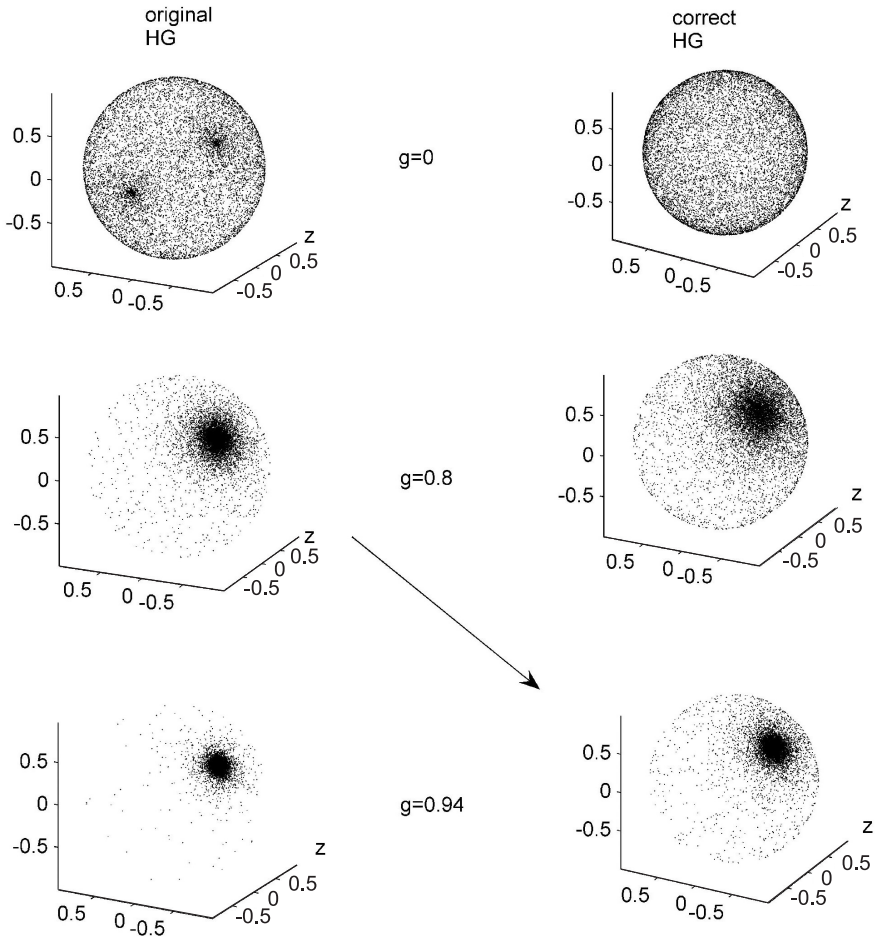

Fig. 3. Projections of photons directions after scattering event on a unit sphere. Results of simulations carried out using the original $c(\phi)$ phase function (left panel) and the analytical inversion $c_a(\phi)$ (right panel). Incident direction is parallel to z axis and scattering occurs at the origin. Results of simulations obtained for isotropic scattering $g = 0$ (upper row), anisotropic scattering $g = 0.8$ (middle row) and $g = 0.94$ (lower row)

Anisotropic scattering photon direction density is presented in the middle and lower rows of Fig. 3. Arrow connecting two distributions indicates the similar distributions obtained by both the methods of phase function sampling but with the use of different anisotropy coefficients. To obtain similar distributions of scattering angles, the value $g_a = 0.9406$ should be used in the case of numerical inversion of the original HG phase function instead of $g = 0.8$.

The differences between the respective functions presented in Fig. 2 can be minimized if the g value used in the analytical expression $c_a(\phi)$ is corrected. An example of such correction is given in Fig. 4A, where the distributions of the cosine of polar

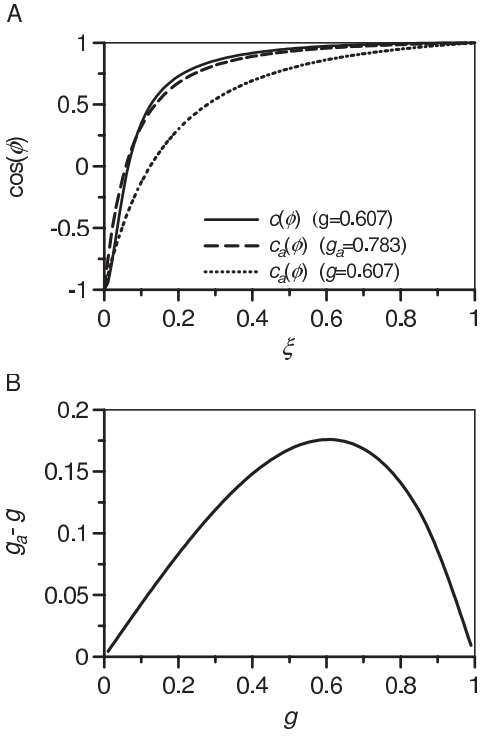

Fig. 4. A: Cosine distributions obtained using different methods of calculation. Numerical calculation based on $c(\phi)$ (eqns. 5, 8) for $g = 0.607$ – solid line; analytical inversion $c_a(\phi)$ (eq. 7) for $g = 0.607$ – dotted line, fitted analitycal $c_a(\phi)$ (eq. 7) to sampled numerical inversion for $g = g_a = 0.783$ – dashed line; B : differences between the anisotropy coefficient g and the corrected anisotropy coefficient g_a in the analytical inversion $c_a(\phi)$ (eq. 7) where g_a is the value of the anisotropy coefficient at the smallest root mean square error smaller than in the case of the numerical inversion $c(\phi)$ (eqns. 5, 8)

deflection angle are shown for the different methods used. The solid line represents the cosine distribution for $g = 0.607$ calculated by numerical inversion of cumulative distribution of the original HG phase function $c(\phi)$, the dashed line corresponds to analytical inversion $c_a(\phi)$ calculated for the same anisotropy coefficient $g = 0.607$, the dotted line is the distribution of the cosine obtained by analytical inversion $c_a(\phi)$ for $g_a = 0.783$. The g_a value is that for which a minimum of the root mean square error of the difference between the cosine from analytical $c_a(\phi)$ and numerical $c(\phi)$ inversion of cumulative distribution of original HG phase function is obtained. In Fig. 4B the difference between the original g value and the corrected g_a value is presented as a function of g. It can be observed that for low and high g values the difference between original and corrected g is small.

The function presented in Fig. 4B can be well approximated by the log-normal function of the following form:

$$g_a \approx g + a + b\exp\left(-\frac{\ln(2)}{\ln^2(e)}\ln^2\left(\frac{(g-c)(e^2-1)}{de}+1\right)\right) \tag{9}$$

with parameters: $a = -1.895$, $b = 2.072$, $c = 0.607$, $d = 3.416$, $e = 0.294$. This function gives maximum error of the corrected anisotropy coefficient g not greater than 0.00167.

The root mean square error between the cosine calculated by analytical expression $c_a(\phi)$ and the cosine calculated by numerical calculation of $c(\phi)$ is defined as:

$$r = \frac{1}{N}\sqrt{\sum_{i=1}^{N}\left(c(\phi)-c_a(\phi)\right)^2}\,, \tag{10}$$

where N is a number of samples. This error versus anisotropy coefficient is shown in Fig. 5 as a dotted line. The root mean square error for g_a after correction of the anisotropy coefficient is much smaller. (see Fig. 5 – solid line).

We tested influence of the method of the phase function calculation on the results of simulations carried out for a homogeneous medium with optical properties similar to those of living tissues (reduced scattering coefficient: $\mu_s = 2\text{cm}^{-1}$ and absorption coefficient $\mu_a = 0.1\text{cm}^{-1}$, anisotropy coefficient $g = 0.8$, refractive index $n = 1.4$ [9, 28]).

The Monte Carlo simulations were performed for different source-detector separations. On this basis, the spatial distributions of the visiting probabilities were obtained. The 2-dimensional projections of the visiting probability distributions are shown in Fig. 6. Distributions of the visiting probability presented in column A were obtained using the original MCML code, i.e. by the analytical inversion $c_a(\phi)$. The distributions shown in column B in Fig. 6 were obtained by the numerical inversion of cumulative distribution of the original HG phase function $c(\phi)$. For the distribu-

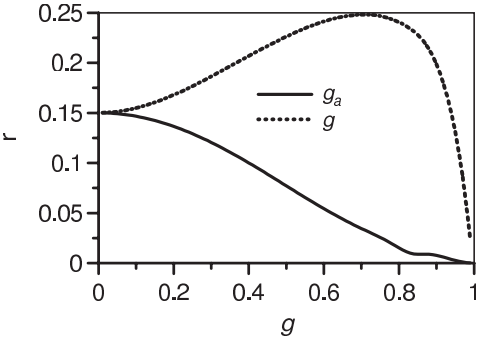

Fig. 5. Root mean square error as a function of the anisotropy coefficient g in the case of the analytical inversion of the cosine of polar deflection angle $c_a(\phi)$ (eq. 7) and of the numerical inversion $c(\phi)$ (eqns. 5, 8) for the same anisotropy coefficient – dotted line; for the corrected anisotropy coefficient g_a – solid line

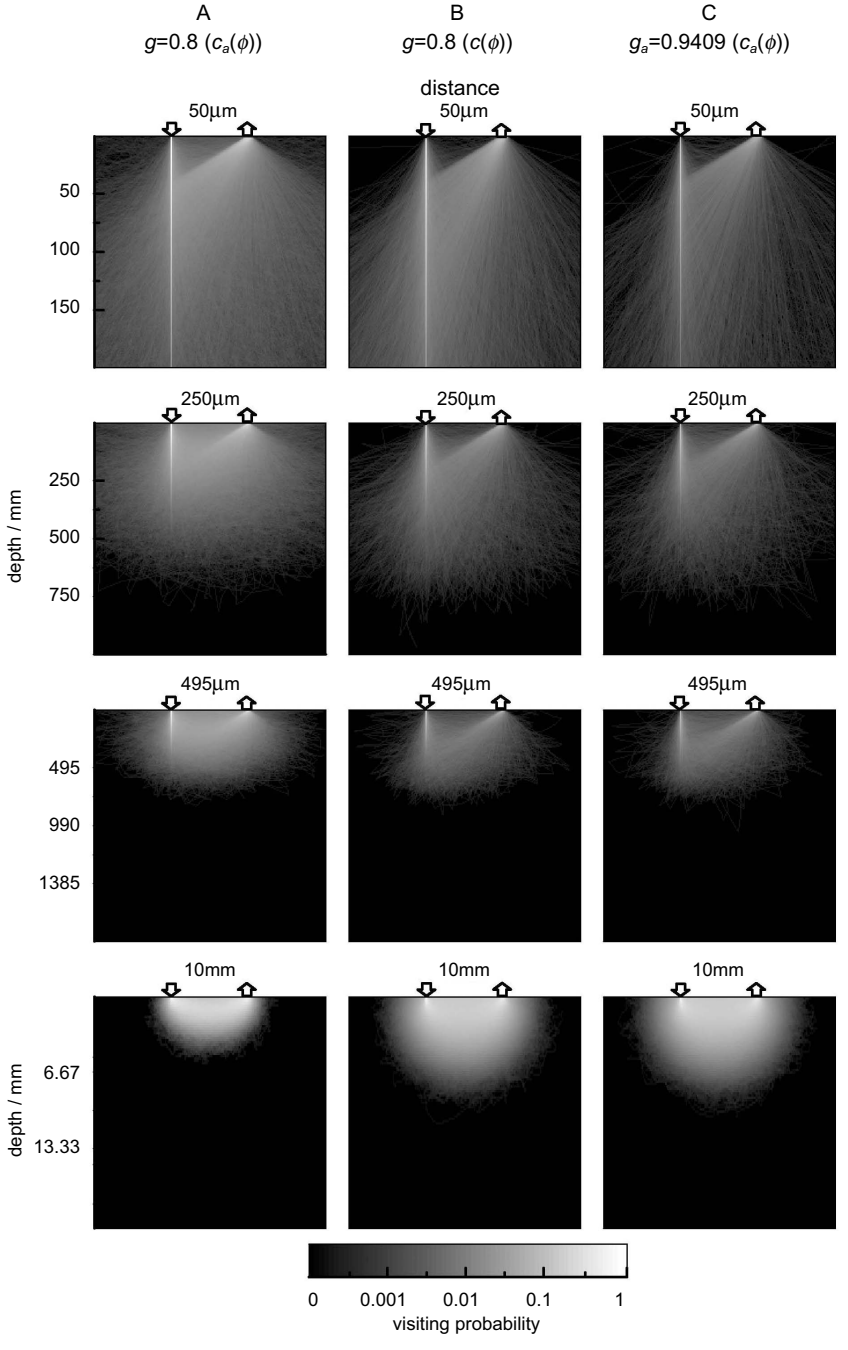

Fig. 6. Photon package visiting probability: first row panels: 50μm, second row panels: 250μm, third row panels: 495μm, fourth row panels: 10mm. A. optical properties: $\mu_s = 2\text{cm}^{-1}$, $\mu_a = 0.1\text{cm}^{-1}$, $g = 0.8$, distributions obtained using the analytical inversion $c_a(\phi)$; B. optical properties: $\mu_s = 10\text{cm}^{-1}$, $\mu_a = 0.1\text{cm}^{-1}$, $g = 0.8$ distributions obtained using the numerical inversion $c(\phi)$; C. optical properties: $\mu_s = 10\text{cm}^{-1}$, $\mu_a = 0.1\text{cm}^{-1}$distributions obtained using the analytical inversion $c_a(\phi)$ with the corrected anisotropy factor $g_a = 0.9406$

tions presented in column C, the calculations were performed using the analytical inversion $c_a(\phi)$ and the original MCML code with corrected anisotropy coefficient g_a. Rows in Fig. 6 represent different source detector separations (row 1 – 50μm, 2 – 250μm, 3 – 450μm, 4 – 10mm). The detection ring was 0.5mm thick in the last case. The scattering coefficient was $\mu_s = 10\text{mm}^{-1}$ and the anisotropy coefficient was 0.8. The corrected anisotropy coefficient in the case C (Fig. 6), calculated according to the formula (eq. 9), was $g = 0.9406$.

More quantitative comparison of the properties of visiting probability distributions obtained by the different methods of the phase function calculation is presented in Figs. 7 and 8. In Fig.7, the reflectance *versus* the source-detector distance is presented. The solution of diffusion equation [13] was compared with the results of the Monte Carlo simulations performed by the analytical inversion of the phase function $c_a(\phi)$ as well as with the results of simulations obtained by the numerical inversion of cumulative distribution of the original HG phase function $c(\phi)$ for isotropic scattering ($g = 0$). It can be observed that the results of the Monte Carlo simulations do not agree with the solution of diffusion equation for the short source-detector distances. Furthermore, for very short source-detector distances, the difference can be observed between the results of the Montre Carlo simulations carried out for different methods of the phase function calculations.

In Fig. 8, feasibility of the proposed correction algorithm is presented. Here the results obtained for anisotropic scattering ($g = 0.8$) calculated with the use of analytical expression $c_a(\phi)$ were compared with those obtained by the numerical inversion of cumulative distribution of the original HG phase function $c(\phi)$. The difference between the reflectance obtained for these methods of phase function calculation is large. We calculated also the reflectance using the analytical inversion $c_a(\phi)$ with corrected anisotropy coefficient $g_a = 0.9406$. In this case, the reflectance agrees well with the data obtained for the numerical inversion of cumulative

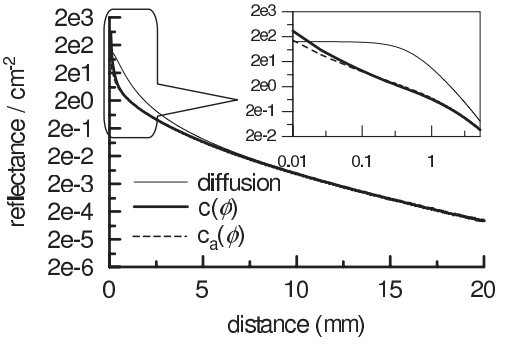

Fig. 7. Reflectance as a function of source-detector separation for semi infinite homogeneous medium with optical properties: $\mu_s = 20\text{cm}^{-1}$, $\mu_a = 0.1\text{cm}^{-1}$, $g = 0$, obtained using the analytical inversion $c_a(\phi)$ – dashed line; the numerical inversion $c(\phi)$ – bold solid line, and solution of diffusion equation – thin solid line

distribution of the original HG phase function $c(\phi)$ with $g = 0.8$. This result is consistent with the discussed above differences between the visiting probability distributions.

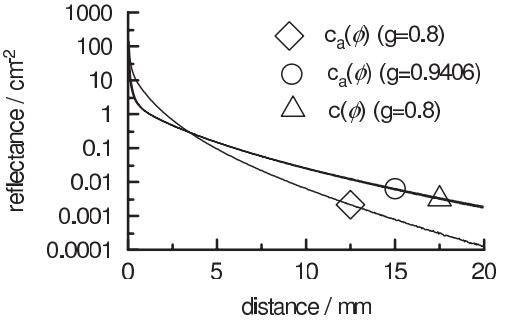

Fig. 8. Reflectance as a function of source-detector distance for semi infinite homogeneous medium with optical properties: $\mu_s = 10\text{cm}^{-1}$, $\mu_a = 0.1\text{cm}^{-1}$, obtained using the analytical inversion $c_a(\phi)$ ($g = 0.8$) – ◇; the numerical inversion $c(\phi)$ (g = 0.8) – △, and the analytical inversion for corrected anisotropy factor $c_a(\phi)$ (g = 0.9406) – ○

5. Discussion and Conclusions

The differences between the distributions of the cosine of polar deflection angle (Fig. 2) lead to the differences in distributions of the visiting probability (Fig. 6 columns A and B). For short source-detector separations considered here, the classical symmetric banana shape of the visiting probability distributions is distorted, and there is no symmetry along the perpendicular bisector of the source-detector segment. The differences are visible in the distributions of the visiting probabilities obtained by the numerical inversion of cumulative distribution of the original HG phase function $c(\phi)$ and the analytical expression $c_a(\phi)$. For the numerical inversion of cumulative distribution of the original HG phase function the probability that the photons penetrate near the surface between the location of the source and the detector is low. On the contrary, when the analytical expression is used, the probability of penetration below the surface is much higher.

The influence of the differences between both the presented methods of computation is best visible in the Monte Carlo simulations carried out for a small source-detector separation, where anisotropy cannot be neglected [29]. These differences tend to disappear when the interoptode distance increases (Fig. 6 bottom panel).

For larger source-detector separations, where photons are diffusively scattered (Fig. 6–4-th row), the visiting probability distributions become symmetrical and form the classical "banana" shape. At large source-detector separations, the consideration of the non-isotropic scattering can be reduced by introduction of a combined measure of the scattering properties of the corresponding isotropic medium, i.e. by the

analysis of reduced scattering coefficient ($\mu_s = (1 - g)\mu_s$). However, the numerical calculation of the polar deflection angle, using the original HG function, can also cause errors in simulations of the large source detection separations with anisotropy of scattering. In this case, the reduced scattering coefficient of the simulated medium becomes erroneous. This effect is visible in Fig. 8.

Tests of speed of the algorithms based on the analytical expression and the numerical inversion of cumulative distribution of the original HG phase function revealed that time of simulations for the numerical inversion with $g = 0.8$ is approximately two times longer than this obtained for the analytical expression with the same anisotropy factor. This effect is caused by the difference in effective g used in both the simulations, i.e. by the difference in reduced scattering coefficient. Comparison of the time needed for simulations in the case of analytical expression with corrected anisotropy factor $g = 0.9406$ and of numerical inversion with $g = 0.8$ shows that speed of the both algorithms is similar. A small difference (about 5%) observed can be caused by faster reading of the cosine of polar deflection angle from look-up table. The same speed for the both algorithms can be also observed for isotropic scattering ($g = 0$).

The error caused by the numerical calculation $c(\phi)$ performed on the basis of the original HG function can be minimized by correcting the anisotropy coefficient using equation (9). Results of such a correction are shown in Fig. 3, in column C in Fig. 6 and in Fig. 8. The differences between the distributions shown in columns B and C in Fig. 6 are difficult to distinguish – only a smaller number of photons was detected in the case C; it is due to the high anisotropy coefficient ($g = 0.9406$). That means that the distributions are more noisy.

The presented recalculation method of the anisotropy coefficient can be easily used to estimate the mean cosine of the scattering angle when the numerical inversion of cumulative distribution of the original HG phase function is applied. It also allows to compare results obtained with application of different methods of calculation of the polar deflection angle.

The data obtained show the influence of the phase function sampling algorithm on the results of the Monte Carlo simulations. The presented approach can be useful in development of the Monte Carlo codes for analysis of the light distributions at short source-detector separations. It may also lead to optimization of optical probe arrangements in the case of applications with small source-detector distances [30–33], e.g. the laser-Doppler blood perfusion measurements or the endoscopic optical measurements.

Acknowledgments

Authors would like to thank prof. R. Maniewski (Institute of Biocybernetics and Biomedical Engineering of the Polish Academy of Sciences) for his comments to the manuscript of the article. This study has been partly supported by research projects number 3T11E01530 and P-N/012/2006 (German-Polish bilateral research project in wavesciences) financed by the State Committee for Scientific Research of the Republic of Poland.

References

1. Maarek J.M., Jarry G., Cosnac B. d., Lansiart A., Mong H.B.: A simulation method for the study of laser transillumination of biological tissues. Ann. Biomed. Eng. 1984, 12, 3, 281–304.
2. Flock S.T., Patterson M.S., Wilson B.C., Wyman D.R.: Monte carlo modeling of light propagation in highly scattering tissue--i: Model predictions and comparison with diffusion theory, IEEE Trans. Biomed. Eng. 1989, 36, 12, 1162–1168.
3. Okada E., Firbank M., Schweiger M., Arridge S.R., Cope M., Delpy D.T.: Theoretical and experimental investigation of near-infrared light propagation in a model of the adult head. Appl. Opt. 1997, 36, 21–31.
4. Steinbrink J., Wabnitz H., Obrig H., Villringer A., Rinneberg H.: Determining changes in nir absorption using a layered model of the human head. Phys. Med. Biol. 2001, 46, 879–896.
5. Mul F.F. M. d., Steenbergen W., Greve J.: Doppler monte carlo simulations of light scattering in tissue to support laser-doppler perfusion measurements. Technology and Health Care 1999, 7, 2–3, 171–183.
6. Liebert A., Wabnitz H., Steinbrink J., Obrig H., Moller M., Macdonald R., Villringer A., Rinneberg H.: Time-resolved multidistance near-infrared spectroscopy of the adult head: Intracerebral and extracerebralabsorption changes from moments of distribution of times of flight of photons. Applied Optics 2004, 43, 15, 3037–3047.
7. Bevilacqua F., Depeursinge C.: Monte carlo study of diffuse reflectance at source-detector separations close to one transport mean free path. J. Opt. Soc. Am. 1999, A 16, 12, 2935–2945.
8. Kienle A., Patterson M.S.: Determination of the optical properties of turbid media from single monte carlo simulation, Phys. Med. Biol. 1996, 41, 2221–2227.
9. Okada E., Delpy D.: Near-infrared light propagation in an adult head model. I. Modeling of low-level scattering in the cerebrospinal fluid layer. Applied Optics 2003, 42, 16, 2906–2914.
10. Pifferi A., Taroni P., Valentini G. and Anderson-Engels S.: Real-time method for fitting time resolved reflectance and transmittance measurements with a monte carlo model. Appl. Opt. 1998, 37, 13, 2774–2780.
11. Swartling J., Pifferi A., Enejder A.M.K., Anderson-Engels S.: Accelerated monte carlo models to simulate fluorescence spectra from layered tissues. J. Opt. Soc. Am. 2003, 20, 4, 714–727.
12. Hielscher A.H., Alcouffe R.E. and Barbour R.L.: Comparison of finite-difference transport and diffusion calculations for photon migration in homogeneous and heterogeneous tissues. Phys. Med. Biol. 1998, 43, 1285–1302.
13. Patterson M.S., Chance B., Wilson B.C.: Time resolved reflectance and transmittance for the noninvasive measurements of tissue optical properties. Appl. Opt. 1989, 28, 12, 2331–2336.
14. Hyde D.E., Farrell T.J., Patterson M.S. and Wilson B.C.: A diffusion theory model of spatially resolved fluorescence from depth-dependent fluorophore concentrations. Phys. Med. Biol. 2001, 46, 369–383.
15. Arridge S.R., Cope M., Delpy D.T., The teoretical basis for the determination of optical pathlengths in tissue: Temporal and frequency analysis. Phys. Med. Biol. 1992, 37, 1531–1560.
16. Liebert A., Wabnitz H., Obrig H., Erdmann R., Möller M., Macdonald R., Rinneberg H., Villringer A. and Steinbrink J.: Non-invasive detection of fluorescence from exogenous chromophores in the adult human brain. Neuroimage 2006, 31, 2, 600–608.
17. Liebert A., Zolek N., Maniewski R.: Decomposition of a laser-doppler spectrum for estimation of speed distribution of particles moving in an optically turbid medium: Monte carlo validation study. Phys. Med. Biol. 2006, 51, 5737–5751.
18. Henyey L.G., Greenstein J.L.: Diffuse radiation in the galaxy. American Astronomical Society 1941, 93, 70–83.
19. VanGemert M.J.C., Jacques S.L., Sterenborg J.C.M., Star W.M.: Skin optics. IEEE Trans. Biomed. Eng. 1989, 36, 12, 1146–1154.

20. Jacques S., Alter C., Prahl S.: Angular dependence of helium-neon laser light scattering by human dermis. Lasers Life Sci. 1987, 4, 309–333.
21. Robert C.P., Casella G.: Monte carlo statistical methods. Springer Verlag, New York, 2004.
22. Binzoni T., Leung T.S., Gandjbakhche A.H., Rufenacht D., Delpy D.T.: The use of the henyey-greenstein phase function in monte carlo simulations in biomedical optics. Phys Med Biol 2006, 51, 17, N313–322.
23. Żołek N.S., Liebert A., Maniewski R.: Optimization of the monte carlo code for modeling of photon migration in tissue. Computer Methods & Programs in Biomedicine 2006, 84, 50–57.
24. Witt A.N.: Multiple scattering in reflection nebulae i. A Monte Carlo Approach. Astrophys. J. 1977, S35, 1–6.
25. Wang L., Jacques S.L.: "Monte carlo modeling of light transport in multi-layered tissues in standard c," University of Texas Texas, 1992.
26. Wang L., Jacques S.L., Zheng I.: Mcml – monte carlo modeling of light transport in multi-layered tissues, Computer Methods & Programs in Biomedicine 1995, 47, 131–146.
27. Bresenham J.E.: Algorithm for computer control of a digital plotter. IBM Systems Journal 1965, 4, 1, 25–30.
28. Bolin F.P., Preuss L.E., Taylor R.C., Ference R.J.: Refractive index of some mammalian tissues using a fiber optic cladding method. Applied Optics 1989, 28, 12, 2297–2303.
29. Spott T.: "Characterization of layered tissue structures with diffusely propagating photon – density waves," Faculty of Electrical Engineering and Telecomunications. Department of Physical Electronics. PhD thesis, Norwegian University of Science and Technology, Trondheim 1999.
30. Mourant J.R., Bigio I.J., Jack D.A., Johnson T.M., Miller H.D.: Measuring absorption coefficients in small volumes of highly scattering media: Source-detector separations for which path lengths do not depend on scattering properties. Appl. Opt. 1997, 36, 5655–5661.
31. Kumar G.: Optimal probe geometry for near-infrared spectroscopy of biological tissue. Appl. Opt. 36 (1997), 2286–2293.
32. Liu H.: Unified analysis of the sensitivities of reflectance and path length to scattering variations in a diffusive medium. Appl. Opt. 2001, 40, 1742–1746.
33. Saager R.B., Berger A.J.: Direct characterization and removal of interfering absorption trends in two-layer turbid media. J. Opt. Soc. Am. A 2005, 22, 1874–1882.